# Quasi-Elastic Light Scattering Studies of Native Hepatic Bile from the Dog: Comparison with Aggregative Behavior of Model Biliary Lipid Systems†

N. A. Mazer,* P. Schurtenberger, M. C. Carey, R. Preisig, K. Weigand, and W. Känzig

ABSTRACT: Using quasi-elastic light scattering (QLS), we have characterized the macromolecular components in hepatic bile obtained from the dog and compared these results with data from model bile solutions containing the bile salt (BS) sodium taurocholate (TC), egg lecithin (L), and cholesterol (Ch). Native bile samples were obtained by direct catheterization of the common bile duct in a previously cholecystectomized dog fitted with a Thomas duodenal cannula. Hepatic bile was sampled during three secretory states: (A) unstimulated "fasting" bile, (B) "stimulated" secretion during an intravenous TC infusion, and (C) "secretin-stimulated" secretion. All three samples had comparable molar ratios of L/BS (0.21 ± 0.03) and Ch/L (0.027 ± 0.006) but differed in the total lipid concentration (BS + L + Ch): (A) 13.1 ± 0.8, (B) 6.7 ± 0.8, and (C) 3.0 ± 0.4 g/dL. From the QLS autocorrelation functions measured on samples B and C, three macromolecular components (denoted $1\alpha$, $1\beta$, and 2) were resolved. Component $1\alpha$ (hydrodynamic radius $R_{1\alpha} = 10 \pm 2$ Å) is comparable in size to the micellar aggregates of model systems. Component $1\beta$ ($R_{1\beta} = 67 \pm 7$ Å) appears to reflect an average of biliary proteins. Component 2 ($R_2 = 650 \pm 15$ Å) is a trace component whose size and sedimentation behavior are compatible with those of the canalicular membrane vesicles postulated to be present in bile [Godfrey, P. P., Warner, M. J., & Coleman, R. (1981) *Biochem. J. 196*, 11]. Serial dilution of the B and C bile samples with Tris buffer (0.15 M NaCl, pH 8.0) showed a remarkable similarity in the behavior of the $1\alpha$ component as compared to the mean hydrodynamic radius $\bar{R}_h$ of similarly diluted model bile solutions. When a critical dilution factor, $d_\gamma$, is reached, $\bar{R}_h$ increases abruptly from ~30 to ~400 Å. Above a second dilution factor, $d_\alpha$, it then decreases to a value of ~150 Å. Similar results were obtained on sample A but were shifted to higher dilutions. Such behavior is consistent with the presence of "mixed disk" micelles [Mazer, N. A., Benedek, G. B., & Carey, M. C. (1980) *Biochemistry 19*, 601] in native bile which undergo a micelle-to-vesicle transition upon dilution. From the $d_\gamma$ and $d_\alpha$ values, estimates of the intermicellar bile salt concentrations were made for all three samples (range 1.4–6.2 mM) which agree well with previous experimental results on model and native bile. These studies offer compelling evidence for the existence of micellar aggregates in native bile whose size, structure, and equilibria are similar to those found in model bile solutions.

On the basis of the striking pathophysiologic correlations demonstrated between the phase equilibria of aqueous biliary lipid systems and the biliary lipid compositions of native bile obtained from man and other species (Admirand & Small, 1968; Redinger & Small, 1972; Holzbach et al., 1973; Carey & Small, 1978), it has generally been inferred that bile salts (BS),[1] lecithin (L), and cholesterol (Ch) form mixed micellar aggregates in native bile with properties similar to those formed in the model systems (Carey & Small, 1970, 1978). Although a number of previous attempts have been made to characterize such aggregates in native bile [see review by Carey & Small (1970)], many of the earlier results were obtained by using conventional techniques (i.e., electrophoresis, gel chromatography, gradient centrifugation, and negative staining electron microscopy) that can seriously perturb micellar equilibria and/or alter aggregate structure. Moreover, as little information on the micellar properties of model bile systems was available at the time of the earlier studies, a detailed comparison between the aggregate structures in native and model bile has never been made previously.

Due to its nonperturbing nature, the technique of quasi-elastic light scattering (QLS) has in recent years become widely applied to the study of micellar systems [see review by Mazer (1984)] and in particular has been used to systematically investigate aqueous biliary lipid systems. In previous work we have employed QLS to characterize (1) the size, shape, thermodynamics, and interactions of bile salt micelles (Mazer et al., 1979a; Schurtenberger et al., 1983a), (2) the structure and equilibria of mixed micelles and vesicles in bile salt–lecithin systems (Mazer et al., 1980; Schurtenberger & Mazer, 1981; Schurtenberger et al., 1983b), and (3) cholesterol solubilization and precipitation in biliary lipid solutions (Carey et al., 1981; Mazer & Carey, 1983). These studies provide a useful experimental and theoretical framework for investigating the more complex native bile solutions.

In the present[2] work we have used QLS to investigate the distribution of particle sizes in hepatic bile obtained from the dog during carefully controlled conditions of bile secretion (Preisig et al., 1962). This species (*Felix canus*) is known to have extremely low concentrations of cholesterol in its bile (Nakayama, 1969; Wheeler & King, 1972) and thus offers

† From the Laboratorium für Festkörperphysik, Eidgenössische Technische Hochschule, CH-8093 Zürich, Switzerland (N.A.M., P.S., and W.K.), the Department of Medicine, Harvard Medical School, Division of Gastroenterology, Brigham and Women's Hospital, Boston, Massachusetts 02115 (M.C.C.), and the Department of Clinical Pharmacology, University of Berne, Berne, Switzerland (R.P. and K.W.). *Received July 19, 1983; revised manuscript received November 28, 1983.* Supported by the Swiss National Science Foundation (Grant 3.614.80), the National Institutes of Health (Research Grant AM 18559), and a grant from the Cystic Fibrosis Foundation.

* Address correspondence to this author at Sandoz AG, Pharmaceutical Research and Development, CH-4002 Basel, Switzerland.

[1] Abbreviations: BS, bile salt; L, lecithin; Ch, cholesterol; TC, taurocholate; QLS, quasi-elastic light scattering; $\bar{R}_h$, mean hydrodynamic radius; $d$, dilution factor; IMC, intermicellar bile salt concentration; $C(\tau)$, unnormalized autocorrelation function; $R(\tau)$, normalized autocorrelation function; $V$, polydispersity parameter; $q$, magnitude of the scattering wave vector; IgA, immunoglobulin A; Tris, tris(hydroxymethyl)aminomethane; $NaDodSO_4$, sodium dodecyl sulfate.

[2] Portions of this work were presented at the American Gastroenterology Association National Meeting, New York (1981), at the Fourth International Conference on Surface and Colloid Science, Jerusalem (1981), and at the Symposium on Bile Acids held in Gstaad, Switzerland (1981) and were published in abstract form (Mazer et al., 1981).

0006-2960/84/0423-1994$01.50/0 

a native system where bile salt–lecithin interactions should predominate. To compare the aggregative behavior of native bile with model bile of identical biliary lipid composition, we studied the effects of serially diluting both systems in vitro with a physiologic buffer solution, as it was previously known that dilution causes mixed micellar growth and leads to the formation of vesicle structures in bile salt–lecithin solutions (Mazer et al., 1980; Schurtenberger et al., 1983b). By this means a quantitative test for assessing the similarity of micellar structure and equilibria in native and model bile was made possible. In addition, we also studied the influence of centrifugation on native bile as a means for characterizing and separating sedimentable components.

We believe the present investigation demonstrates the utility of the QLS technique for characterizing the macromolecular components of native bile and further that it offers the first detailed comparison of biliary lipid aggregation in native and model systems. The relevance of these results to the mechanisms of bile secretion, fat digestion, and the pathogenesis of lipoprotein X is also presented.

## Experimental Procedures

### *Materials*

*Native Bile Samples.* Hepatic bile was collected on three occasions from a female boxer dog (weight 29 kg) prepared 1 year previously by cholecystectomy and placement of a Thomas duodenal cannula (Thomas, 1941). In each collection three bile samples (designated A, B, and C)[3] were obtained after a 24-h fast, by direct catheterization of the common bile duct. Sample A represented the initial drainage from the biliary tree. Sample B was obtained during the steady-state choleretic response to sodium taurocholate (Calbiochem) infused intravenously in 0.9% saline at a rate of 24 μmol of TC/min. Sample C was collected following the simultaneous infusion of TC and secretin (Kabi Diagnostica, Studsvik, Sweden), the latter given at a rate of 4 IU/min for 10 min. All samples were initially collected in glass tubes that were stored on ice. After aliquots were removed for chemical analysis (see Methods), the remaining bile was transferred into foil-covered vials, capped under argon, and packed in dry ice for rail transport from Bern to Zürich (~2-h duration). Samples were then slowly thawed at room temperature and stored overnight at 4 °C prior to light scattering investigation.

*Model Bile Samples.* Recrystallized sodium taurocholate from Calbiochem (San Diego, CA), grade 1 egg lecithin from Lipid Products (South Nutfield, Surrey, U.K.), and twice recrystallized cholesterol (Fluka, Buchs, Switzerland) kindly provided by Prof. H. G. Weder (ETH, Zürich) were used to make model bile solutions of a desired biliary lipid composition by the method of coprecipitation (Small et al., 1969). After an appropriate amount of each lipid was dissolved in ethanol, the mixture was dried under reduced pressure (Büchi rotavapor) until a constant dry weight was obtained. The necessary amount of 0.15 M NaCl/Tris buffer (pH 8.0) was then added, and the solution was flushed with purified $N_2$, sealed, and incubated for 48 h at room temperature with periodic vortex mixing.

### *Methods*

*Quasi-Elastic Light Scattering.* (*a*) *Instrumentation.* The apparatus for measuring both the intensity and autocorrelation function of the scattered light consisted of an Argon ion laser (Spectra Physics, Model 171), a temperature-controlled scattering cell holder with toluene index matching bath, a digital Malvern autocorrelator (K 7023, 96 channels), and an "on-line" data analysis performed by a Nova 3 computer. Details are given elsewhere (Haller, 1980). In the present study measurements were performed at a scattering angle of 90°, sample temperature of 20 °C, laser wavelength of 5145 Å, and laser power of 200–500 mW (depending on the scattering intensity of the samples).

(*b*) *Dust Removal, Scattering Cells, and Alignment.* Aliquots (0.5 mL) of all samples were centrifuged at 15000*g* for 10 min in acid-washed *cylindrical* quartz scattering cells (8 mm i.d.) in order to sediment dust from solution. With these scattering cells it was not possible to study concentrated native bile samples due to the presence of absorbing pigments which greatly attenuated the incident and scattered light from the center of the cell. For this reason the cylindrical tubes were used only for measurements on "pigment-free" model bile and diluted (4-fold or greater) native bile samples. To study concentrated native bile, the centrifuged samples were transferred into *square* quartz cells that were aligned with respect to the incident beam and detection optics so as to minimize the path length of the incident and scattered light inside the cell.[4] Special care was taken to avoid imaging *reflected light* from the corner of the scattering cell, in order to prevent heterodyne effects (Chu, 1974).

(*c*) *Data Acquisition and Analysis.* For each sample the autocorrelation function $C(\tau)$ computed at 96 equally spaced points, $\tau = T_i, 2T_i, 3T_i, \ldots 96T_i$, was measured at various sampling times $T_i$ ranging from 0.5 to 20 μs. The base-line values $B$ [corresponding to $C(\infty)$] were calculated from the monitor channels of the correlator and corresponded well with the measured values of $C(\tau)$ at large values of $\tau$.

Two data analysis approaches were used to obtain information about the distribution of diffusion coefficients associated with the sample. In all cases, a first-, second-, and third-order cumulants analysis (Koppel, 1972) was performed on the first 48 points of each autocorrelation function. From the cumulants, the mean diffusion coefficient $\bar{D}$, polydispersity index $V$, and skewness parameter $S$ were computed as described by Missel et al. (1980). From $\bar{D}$, the apparent mean hydrodynamic radius of the particles was calculated in analogy with the Stokes–Einstein relation:

$$(\bar{R}_H) = \frac{k_B T}{6\pi\eta\bar{D}} \quad (1)$$

where $k_B$ is Boltzmann's constant, $T$ is the absolute temperature, and $\eta$ is the *solvent* viscosity (taken to be the same as in 0.15 M NaCl for both model and native bile samples). The theoretical rationale for this equation has been discussed at length previously (Mazer et al., 1976, 1977; Schurtenberger et al., 1983a). In cases where marked polydispersity was observed ($V > 100\%$), the cumulants showed a strong dependence on sampling time ($T_i$), and a second data analysis approach was employed. In this method correlation functions measured at various $T_i$ values were mathematically "spliced" together (as described in Appendix A) to give a normalized correlation function $R(\tau)$ which decayed from unity to near zero at large $\tau$ values. $R(\tau)$ was then analyzed by a nonlinear least-squares fitting program (Bevington, 1969) which assumed a three-component distribution:

$$R(\tau)^{1/2} = G_1 e^{-D_1 q^2 \tau} + G_2 e^{-D_2 q^2 \tau} + (1 - G_1 - G_2) e^{-D_3 q^2 \tau} \quad (2)$$

with diffusion coefficients $D_1$, $D_2$, and $D_3$ and relative inten-

[3] In certain cases, the subscript 1, 2, or 3 has been applied to these sample names to designate the particular bile collection (see Table I).

[4] A similar scattering geometry was employed by Sanders & Cannell (1980) to study hemoglobin solutions.

Table I: Chemical Analysis of Bile Samples

| sample[a] | mM | | | molar ratio | | g/dL | | | mequiv/L | | | |
|---|---|---|---|---|---|---|---|---|---|---|---|---|
| | BS | L | CH | L/BS | CH/L | total lipids[b] | bilirubin[c] | protein | Na | Cl | K | pH |
| collection 1 | | | | | | | | | | | | |
| $A_1$ | 228.3 | 54 | 1.1 | 0.24 | 0.020 | 12.6 | | 0.34 | 170.5 | 14.3 | 6.6 | |
| $B_1$ | 112.7 | 20 | 0.59 | 0.18 | 0.030 | 7.6 | | 0.22 | 154 | 55.3 | 4.95 | |
| $C_1$ | 59.6 | 12.5 | 0.45 | 0.21 | 0.036 | 4.2 | | 0.18 | 137.5 | 67.4 | 3.85 | |
| collection 2 | | | | | | | | | | | | |
| $A_2$ | 186 | 49 | 1.21 | 0.26 | 0.025 | 13.7 | 0.33 | 0.37 | 252 | 5.75 | 9.75 | 7.23 |
| $B_2$ | 96 | 19.9 | 0.58 | 0.21 | 0.029 | 6.7 | 0.11 | 0.41 | 200 | 26.0 | 6.75 | 8.0 |
| $C_2$ | 51 | 11.42 | 0.33 | 0.22 | 0.029 | 3.6 | 0.07 | 0.27 | 187 | 32.35 | 6.15 | 8.11 |
| collection 3 | | | | | | | | | | | | |
| $B_3$ | 89.8 | 14.11 | 0.265 | 0.16 | 0.019 | 5.9 | 0.07 | 0.53 | 183 | 55.5 | 6.2 | |

[a] Samples are denoted as A, B, or C (see Methods) with subscripts that refer to the particular collection. [b] Refers to total concentration of bile salt, lecithin, and cholesterol. [c] Refers to total concentration of conjugated species.

sities $G_1$, $G_2$, and $(1 - G_1 - G_2)$, respectively. The fitting program allowed any of the five parameters ($D_1$, $D_2$, $D_3$, $G_1$, and $G_2$) to be either fixed or kept free and thus permitted "two-component fits" ($G_2 = D_2 = 0$), "amplitude fits" ($D_1$, $D_2$, and $D_3$ specified), and other variations to be readily made. The apparent hydrodynamic radii of the individual components, $R_i$, were calculated from the $D_i$ values using eq 1.

*Chemical Analysis of Native Bile.* Total bile salt and phospholipid concentrations were determined from whole bile by using standard methods (Paumgartner et al., 1971; Bartlett, 1959). Biliary cholesterol was extracted in chloroform–methanol (2:1) and then measured with a commercial assay (Cholesterol Test, Roche, Basel). Sodium and potassium concentrations were measured by flame spectrophotometry, chloride concentration by the method of Cotlove et al. (1958), and bile pH using an Orion pH meter. The total bilirubin concentration was determined by the method of Michaëlsson et al. (1965).

Biliary protein was precipitated by trichloroacetic acid, redissolved in 0.5 N NaOH, and measured by the method of Lowry et al. (1951). As standard, bovine serum albumin was used to which deproteinized dog bile (kept in the dark) had been added. The presence of serum albumin and IgA in bile was determined by electroimmunodiffusion (Laurell, 1966) using monospecific antisera (Miles-Yeda Ltd., Israel). Dog albumin, purified as described previously (Weigand et al., 1982), served as standard for the albumin determination. Since no pure dog IgA was available, serially diluted dog serum (from the same animal) was used as standard and the IgA content of bile compared with that of serum. A qualitative assessment of biliary proteins was also obtained by NaDod-$SO_4$–polyacrylamide slab gel electrophoresis, according to King & Laemmli (1971).

*Dilution Experiments.* Model and native bile samples were serially diluted with 0.15 M NaCl/Tris (pH 8.0) buffer, by adding aliquots (1 mL) of bile and buffer in a 1/1 ratio, vortex mixing for 10 s, and repeating the procedure successively using 1 mL of the previously diluted sample. To obtain intermediate dilutions, aliquots of bile and buffer with unequal volumes were mixed. In all cases, the entire "dilution series" was prepared in a time of less than 10 min, after which samples were sealed under nitrogen and incubated. For model bile, the incubation was at 20 °C and lasted 48 h [a time sufficient for equilibrium to be reached (Schurtenberger et al., 1983b)]. With native bile samples, the incubation was at 4 °C for a similar length of time. Prior to the light scattering investigation, the native samples were maintained at 20 °C for at least 1 h.

*Centrifugation Experiments.* Aliquots (1 or 4 mL) of native bile (sample $B_3$) were centrifuged in polyethylene tubes (9 or 15 mm i.d., respectively) in a Sorvall RC2-B centrifuge (fixed angle rotor type SS-34) at 20000*g* for varying lengths of time (1–4 h). Although no macroscopic sediments were visible in any of the tubes, care was taken to aspirate the supernatant phases without disturbing the inner walls (or bottoms) of the tubes. The supernatants were then vortex mixed, and 0.5 mL was pipetted into rectangular quartz light scattering cells and the remaining material subjected to chemical analysis. In addition, a 1-mL aliquot of supernatant (4-h centrifugation) was serially diluted and studied as described above.

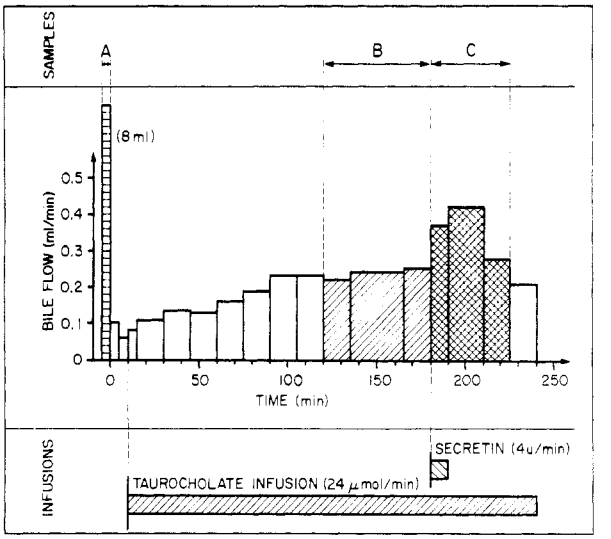


FIGURE 1: Dependence of bile flow vs. time during the collection of bile samples. Sample A represents the initial drainage of bile obtained after catheterizing the animal (and is indicated as a volume, rather than flow). Sample B was collected during the steady-state response to a taurocholate infusion. Sample C was collected during the state of increased bile flow resulting from secretin administration. Data correspond to collection 2 (see Table I).

## Results

*(A) Physiological and Chemical Characterization of Bile Samples.* The three states of hepatic bile secretion in which bile samples were obtained are illustrated in Figure 1. The initial biliary drainage after catheterization, sample A, corresponds to bile that was secreted and concentrated in the biliary tree during the previous 24-h fast. Sample B represents newly secreted bile stimulated by a taurocholate infusion of 24 μmol/min. Sample C corresponds to the state of increased bile flow (Preisig et al., 1962) resulting from secretin administration during the TC infusion.

A chemical characterization of bile samples obtained in all three collections is given in Table I. In contrast to the relative

Table II: Three-Component Light Scattering Analysis of Bile

| sample | component | $D_i$ ($\times 10^{-7}$ cm$^2$ s$^{-1}$)[a] | $R_i$ (Å)[b] | $G_i$ (%)[c] | $W_i$ (%)[d] A | $W_i$ (%)[d] B | $V$ (%)[e] | $S$ (%)[e] |
|---|---|---|---|---|---|---|---|---|
| $B_3$ | 1α | 24.94 | 8.5 | 22.1 | 99.5 | 92.4 | | |
| | 1β | 3.62 | 58.6 | 35.8 | 0.49 | 7.5 | | |
| | 2 | 0.320 | 663 | 42.1 | 0.0004 | 0.028 | | |
| | mean: 1α + 1β + 2 | 6.95 | 30.5 | | | | 139 | 126 |
| $B_2$ | 1α | 22.55 | 9.4 | 25.3 | 99.6 | 92.5 | | |
| | 1β | 3.00 | 70.6 | 40.5 | 0.376 | 7.44 | | |
| | 2 | 0.337 | 628 | 34.2 | 0.0004 | 0.02 | | |
| | mean: 1α + 1β + 2 | 6.07 | 34.9 | | | | 129 | 108 |
| $C_2$ | 1α | 16.96 | 12.5 | 29.1 | 99.4 | 94.5 | | |
| | 1β | 3.00 | 70.6 | 33.6 | 0.638 | 5.49 | | |
| | 2 | 0.334 | 635 | 37.3 | 0.0009 | 0.019 | | |
| | mean: 1α + 1β + 2 | 6.06 | 35.0 | | | | 116 | 84 |

[a] Translational diffusion coefficient of $i$th component (or intensity weighted average of components). [b] Apparent hydrodynamic radius calculated from $D_i$ (eq 1). [c] Fraction of scattered intensity associated with the $i$th component. [d] Fraction of solute concentration calculated from $G_i$ values using eq 3 with two different estimates ($A$, $B$) of molecular weights and form factors (see Appendix B). [e] Variance and skewness computed for 1α + 1β + 2 distributions [see Missel et al. (1980)].

lipid concentrations (L/BS and Ch/L) which are similar for all samples, the total lipid concentration (BS + L + Ch) varies markedly between the three states (sample A > B > C), reflecting differences in the secretion and reabsorption of bile water. The bilirubin and protein concentrations tend to parallel the total lipid concentration but are more than an order of magnitude smaller. Electrolyte composition and pH show some minor variations.

Although not directly measured, it should be expected that the particular bile salt species in sample A will differ from samples B and C. The latter should consist almost entirely of the infused TC, whereas sample A would be representative of the endogenous BS pool, known to contain taurine conjugates of both dihydroxy and trihydroxy bile salts in the dog (Haslewood, 1967; Nakayama, 1969).

With regard to the specific proteins in bile, electroimmunodiffusion analysis of sample $B_3$ showed that albumin and IgA were the major serum proteins present, the latter at a concentration greater than that measured in the dog's serum. Similar results have been reported in the dog (Dive et al., 1974) and rat (Mullock et al., 1978), previously.

*(B) Quasi-Elastic Light Scattering Characterization of Native Bile.* In the case of sample A, the relatively high concentration of bilirubin pigment in undiluted bile (Table I) strongly interfered with light scattering measurements despite our efforts to optimize the scattering cell geometry (see Methods). Nevertheless, with samples B and C it was possible to obtain autocorrelation functions with good signal-to-noise ratios. As an example, Figure 2A illustrates the normalized autocorrelation function $R(\tau)$ from sample $B_3$, obtained by mathematically splicing together data measured at different sampling times (see Appendix A). The marked curvature seen in the semilogarithmic plot of $R(\tau)$ implies that the sample is highly polydisperse. To obtain quantitative information on the particle size distribution, a multiexponential analysis of $R(\tau)$ based on eq 1 was performed. When a two-exponential function was used, systematic deviations were clearly visible, particularly at $\tau$ values < 300 μs (Figure 2B), whereas with a three-exponential function such deviations were undetectable (Figure 2C). Similar results using a three-component analysis were obtained on all B and C samples studied. The diffusion coefficients ($D_i$), hydrodynamic radii ($R_i$), and relative scattering intensities ($G_i$) of the three components are given in Table II. In all samples, the two smaller components, denoted as 1α and 1β, have $R_i$ values of approximately 10 and 67 Å, respectively. The large particles, denoted as component 2, are ~650 Å in size.

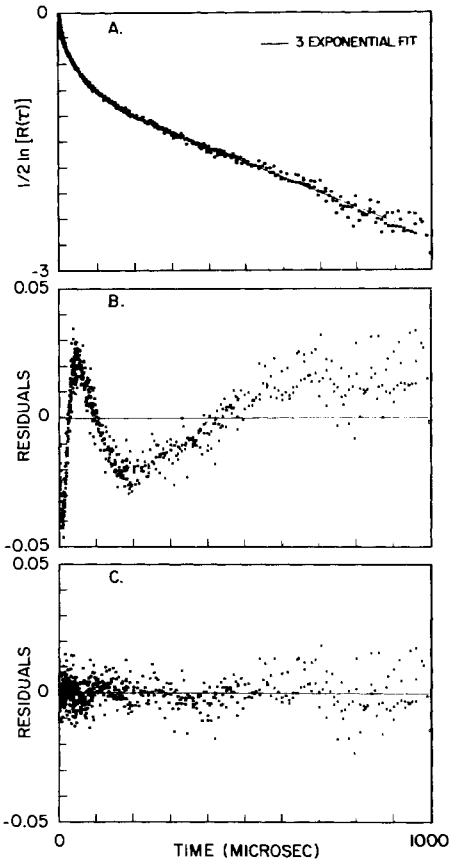


FIGURE 2: (A) Normalized autocorrelation function, $R(\tau)$, obtained from native bile sample $B_3$ and plotted as $^1/_2 \ln [R(\tau)]$ vs. $\tau$. Data were obtained by mathematically splicing together seven autocorrelation functions (596 data points) measured at sampling times of 0.5, 1, 2, 5, 10, 15, and 20 μs (see Appendix A). Solid curve represents a three-exponential fit to $R(\tau)^{1/2}$. (B) Residuals plot for two-exponential fit. (C) Residuals plot for three-exponential fit.

Although the three components have similar $G_i$ values (33 ± 10%), they constitute markedly different fractions ($W_i$) of the total solute concentration (weight/volume). This follows from the relationship between $W_i$ and $G_i$ (Mazer et al., 1976):

$$W_i = \frac{G_i/[M_i P_i(q)]}{\sum G_i/[M_i P_i(q)]} \quad (3)$$

where $M_i$ is the molecular weight and $P_i(q)$ is the scattering form factor of the $i$th component. As a first approximation, we assumed $M_i$ to be proportional to $R_i^3$ (i.e., spherical particles) and took $P_i = 1$ in order to compute the $W_i$ values from

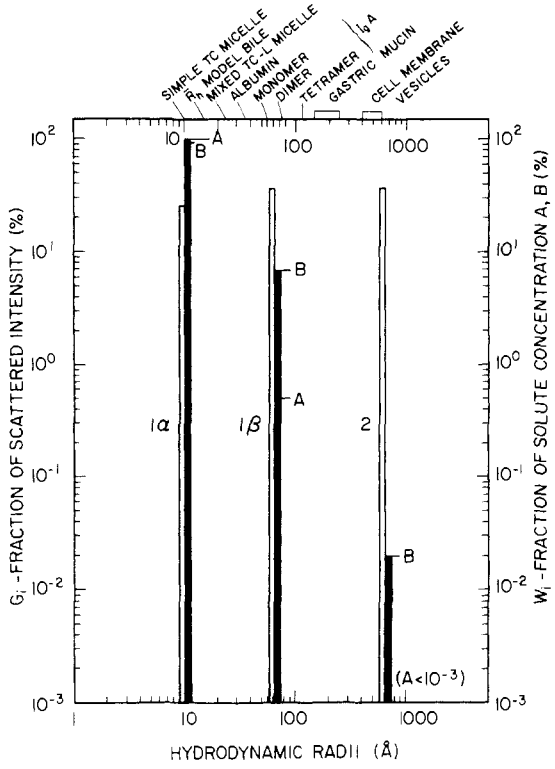


FIGURE 3: Histogram representation of the relative intensities (open columns) and relative solute concentrations (filled columns) for the three-component (1$\alpha$, 1$\beta$, and 2) analysis of bile. Data are obtained by averaging results for samples $B_3$, $B_2$, and $C_2$ (Table II). Relative solute concentrations are computed for cases A and B based on different estimates of the molecular weights and form factors of the components (see Appendix B). Upper abscissa permits comparison of the hydrodynamic radii of components 1$\alpha$, 1$\beta$, and 2 with the hydrodynamic radii of simple TC micelles, mixed TC–L micelles, mean micellar radius, albumin, IgA oligomers, gastric mucin protein, and cell membrane vesicles (see text for explanation).

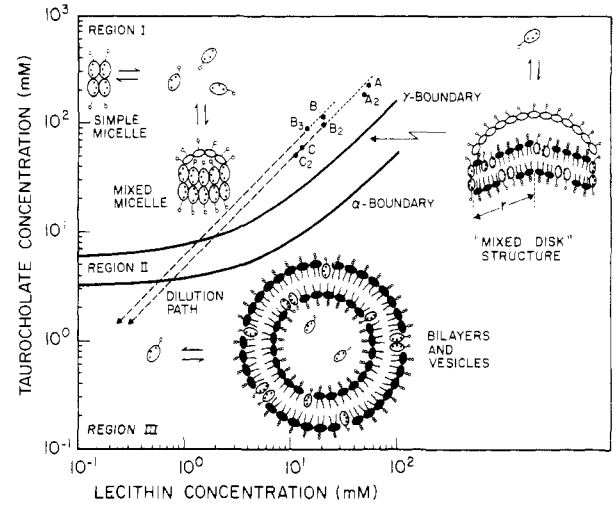


FIGURE 4: Phase diagram and aggregate structures for taurocholate–lecithin model systems (20 °C, 0.15 M NaCl) from Mazer et al. (1980). In region I simple TC micelles and small TC–L mixed micelles coexist above $\gamma$-boundary. In region II mixed disk TC–L micelles exist whose radius ($r$) appears to diverge as the $\alpha$-boundary is approached. In region III bilayers and in dilute solutions unilamellar vesicles are formed. Also plotted are the bile salt/lecithin concentrations corresponding to the seven bile samples given in Table I. These fall in region I of the model system. Dashed lines indicate the path in the phase diagram associated with diluting samples $B_2$ and $B_3$. Dotted lines extend these paths to higher concentrations typical of the A samples. Equilibrium between aggregates and TC monomers is also illustrated.

eq 3. The results are given in Table II (case A) along with a second set of values that employ more rigorous estimates of $M_i$ and $P_i$ (case B, given in Appendix B). Within these limits it is seen that 1$\alpha$ is the major macromolecular component in bile representing 92.4–99.6% of the total solute concentration, that 1$\beta$ is a minor component (0.4–7.5%), and that component 2 is only a trace constituent of bile (<0.028%).

A graphical illustration of the three-component representation is shown in Figure 3, which plots the $G_i$ and $W_i$ values vs. the corresponding $R_i$. Also indicated on the abscissa are the hydrodynamic radii corresponding to simple TC and mixed TC–L micelles (Mazer et al., 1980), serum albumin and IgA (monomer plus oligomers) (Putnam, 1965), gastric mucin glycoproteins (Pearson et al., 1980), and bile salt/cell membrane vesicles (Billington & Coleman, 1978). Comparison of the three components with these species shows that the major biliary component seen by light scattering, 1$\alpha$, is approximately the same size as the simple TC micelle, that 1$\beta$ falls in the range expected for biliary serum proteins, and that component 2 is similar in size to cellular membrane vesicles postulated by Godfrey et al. (1981) to be present in bile. In the following sections further investigations concerning the physicochemical nature of these components are presented.

(*C*) *Characterization of Component 1α: Comparison with Model Biliary Lipid Systems. (1) Micellar Properties of Model Dog Bile.* In view of the very small amounts of cholesterol present in dog bile, it is beneficial to utilize the taurocholate–egg lecithin system as a framework for comparing biliary lipid association in model and native bile. Figure 4 represents the aggregative phenomena occurring in this system in terms of a micellar phase diagram deduced from quasi-elastic light scattering studies (Mazer et al., 1980). When the bile salt/lecithin compositions (Table I) of the A, B, and C bile samples are plotted on the phase diagram, they are all observed to lie in region I, where simple micelles and mixed TC–L micelles coexist in varying proportions.

To compare the previous results on native bile with the light scattering from model systems, we prepared aqueous biliary lipid solutions with TC, L, and Ch concentrations that were identical with those of samples $B_2$ and $B_3$ (see Methods). The autocorrelation functions from these solutions exhibited much less curvature (see Figure 5A) than for native bile and could be adequately analyzed with a second-order cumulants analysis. In both cases the mean hydrodynamic radius was ~15 Å, and polydispersity index V was ~50%, values which are consistent with the coexistence model of region I (Mazer et al., 1980). In addition to the cumulants analysis a two-component representation of the model $B_3$ bile was also obtained (Figure 5C). The two components had comparable scattering intensities, and their hydrodynamic radii were 9.0 and 28.7 Å, close to those expected for simple and mixed micelles (Mazer et al., 1980). While the coexistence model (Figure 4) has recently been questioned (Müller, 1981; Claffey & Holzbach, 1981; Spink et al., 1982), our data show clear evidence of polydispersity and cannot be adequately fit by a single exponential (see Figure 5B).

Although the 1$\alpha$ component of native bile is similar in size to the simple TC micelle, we believe that it most likely represents the combined contributions from both simple and mixed micellar species. This view is consistent with our estimates of $W_{1\alpha}$, which shows that the 1$\alpha$ component contains greater than 90% of the total solute concentration (i.e., comparable to the bile salt plus lecithin concentration). The small difference between $R_{1\alpha}$ (~10 Å) and $\bar{R}_h$ of the model system (~15 Å) is most likely an artifact of our data analysis caused by trying to represent the more complex native bile system with only three components.[5]

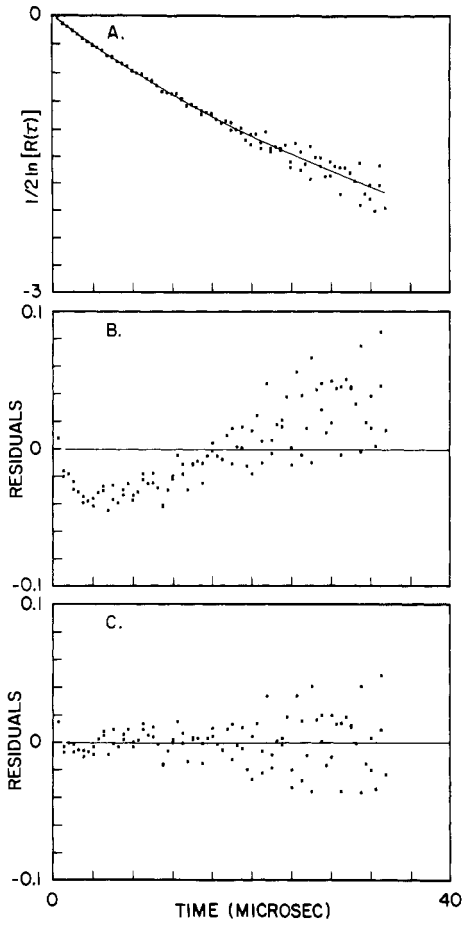


FIGURE 5: (A) Spliced autocorrelation function for model $B_3$ bile plotted as $^1/_2 \ln [R(\tau)]$ for $\tau$ values between 0 and 40 $\mu$s. Solid curve represents two-exponential fit. (B) Residual plot for single-exponential fit shows systematic deviations. (C) Residual plot for two-exponential fit shows random deviations.

*(2) Effects of Dilution on Model and Native Bile.* When the model and native dog bile samples depicted in Figure 4 are serially diluted with an aqueous buffer solution, the resulting biliary lipid concentrations follow linear paths in the phase diagram which pass from region I into regions II and III with increasing dilution. In the TC–L system, region II corresponds to solutions which contain "mixed disk" micelles whose size increases dramatically as the micellar phase limit ($\alpha$-boundary) is approached (Mazer et al., 1980). In region III, insoluble bilayers and/or vesicle structures are formed, the latter occurring in more dilute systems (Schurtenberger et al., 1983b).

Dilution of model dog bile ($B_2$ and $B_3$ samples) produces marked changes in $\bar{R}_h$ (Figure 6), consistent with the TC–L phase diagram. At low dilutions within region I, $\bar{R}_h$ increases from ~15 to 30 Å, a result of the decreasing proportion of TC micelles coupled with an increase in the apparent size of the coexisting TC–L micelles. At the dilution where the $\gamma$-boundary is crossed ($d_\gamma$), $\bar{R}_h$ increases dramatically as expected from the mixed disk model. Theoretically the mixed disk radius, $r$, should increase with dilution factor, $d$, according to (Mazer et al., 1980)

$$r = \left(\frac{2\rho}{\sigma'}\right)\frac{C_L^0}{C_{BS}^0 - \alpha^{-1}C_L^0 - d\cdot\mathrm{IMC}} \qquad (4)$$

[5] In view of the high quality fit of the three-exponential function to our data (Figure 2C) we believe that the use of more components or more sophisticated data analysis techniques [see Ostrowsky & Sornette (1983), Bertero & Pike (1983), and Ford & Chu (1983)] would be unwarranted.

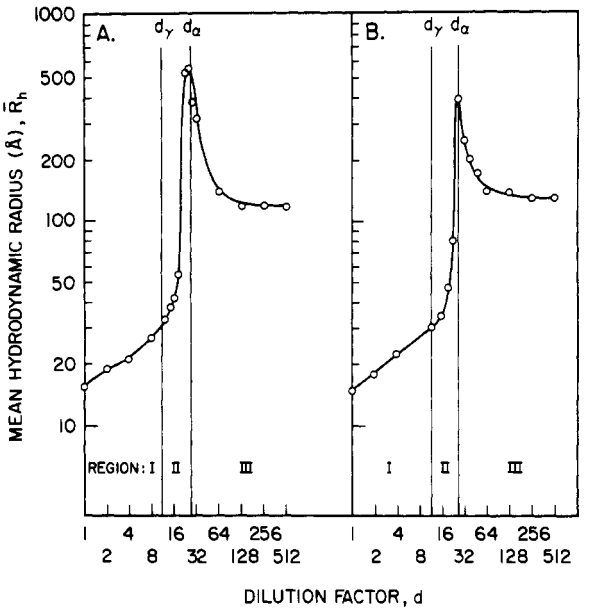


FIGURE 6: Effect of dilution on the mean hydrodynamic radius, $\bar{R}_h$, of model bile systems. (A) Model $B_2$ bile. (B) Model $B_3$ bile. Vertical lines denote critical dilutions, $d_\gamma$ and $d_\alpha$, which mark the crossing of the $\gamma$ and $\alpha$ boundaries of the phase diagram and separate regions I, II, and III (see Figure 4).

where $2\rho/\sigma'$ is a geometric factor, $C_{BS}^0$ and $C_L^0$ represent the initial concentrations of BS and L, and IMC is the intermicellar BS concentration (which lies between $IMC_\gamma$ and $IMC_\alpha$, the respective concentrations at the $\gamma$- and $\alpha$-boundary). Equation 4 actually predicts a divergence in $r(r \to \infty)$ at a critical dilution factor, $d_\alpha$, corresponding to the point at which the dilution path crosses the $\alpha$-boundary. Rather than a true divergence we find experimentally (Figure 6) that $\bar{R}_h$ reaches a maximum value (in the range 400–600 Å) at a dilution close to $d_\alpha$. At higher dilutions the $\bar{R}_h$ values correspond to vesicle structures formed in region III of the phase diagram and exhibit a marked decrease with $d$, approaching a minimum value of 120–130 Å. Thus, a micelle-to-vesicle transition occurs spontaneously in the vicinity of $d_\alpha$ and prevents an actual divergence in $\bar{R}_h$ from occurring[6] (Schurtenberger et al., 1983b).

Figure 7A–C, shows the effect of dilution on native bile samples $B_3$, $B_2$, and $C_2$, respectively. At low dilutions ($1 \lesssim d \lesssim 16$) it was possible to follow the behavior of the separate components ($1\alpha$, $1\beta$, and 2) previously seen in undiluted samples. To within experimental error, the hydrodynamic radii of components $1\beta$ and 2 remained constant over this range, while the fraction of light scattered by them decreased appreciably.[7] In contrast both the size and intensity of the $1\alpha$ component increased steadily, similar to the behavior of the corresponding model system (dashed curves). Above this range of dilution factors (somewhat lower for the $B_2$ and $C_2$ samples) it was not possible to resolve the separate components, and only the mean radius, $\bar{R}_h$, is plotted. It largely reflects the behavior of the $1\alpha$ component and exhibits an abrupt rise and subse-

[6] From recent studies on model systems (Schurtenberger et al., unpublished results) it appears that close to the peak of the $\bar{R}_h$ curve ($d_\alpha \lesssim d \lesssim 1.3d_\alpha$) large mixed micelles and vesicles may coexist whereas at higher dilutions only vesicles are present.

[7] When $R_{1\beta}$ and $R_2$ were held as free parameters in the data analysis they showed only minor fluctuations (±20%) from the values deduced in undiluted samples. In the data analysis presented in Figure 7A–C, $R_{1\beta}$ and $R_2$ were fixed at the latter values, and the parameters $R_{1\alpha}$, $G_{1\alpha}$, and $G_{2\beta}$ were fit by using eq 2. These "fits" had nearly identical $\chi^2$ values when compared to the cases where all five parameters were allowed to vary.

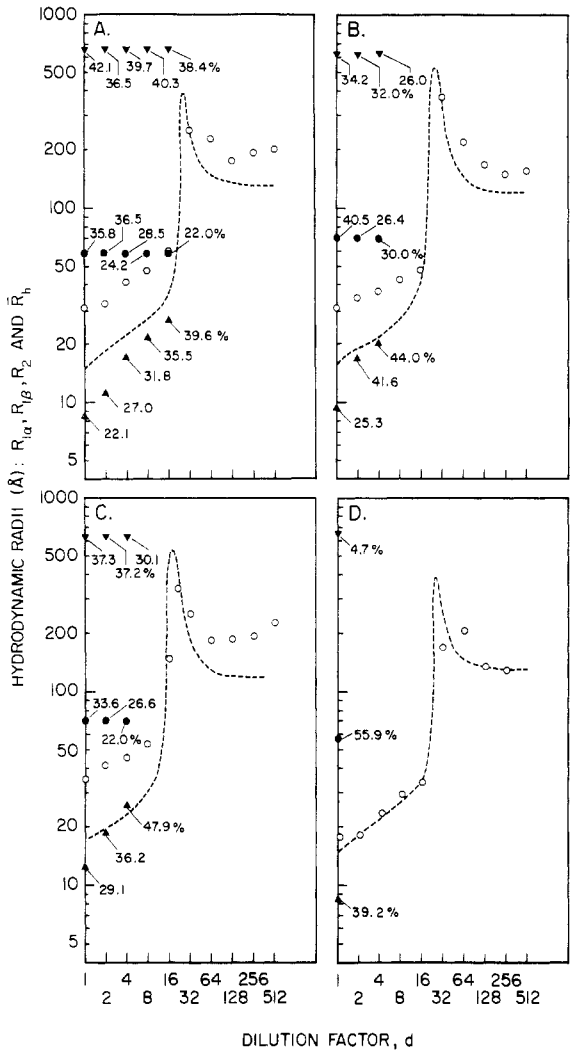


FIGURE 7: Effect of dilution on the hydrodynamic radii of native bile. (A) Sample $B_3$. (B) Sample $B_2$. (C) Sample $C_2$. (D) Sample $CF_4$. At low dilution factors, samples have been resolved into three components whose hydrodynamic radii $R_{1\alpha}$ (▲), $R_{1\beta}$ (●), and $R_2$ (▼) are each shown; together with the respective fractions (%) of the scattered light intensity. At higher dilution factors only the mean hydrodynamic radius $\bar{R}_h$ (○) (derived from a cumulants analysis) is illustrated. The $\bar{R}_h$ values shown at lower dilutions are derived from the three-exponential analysis. Dashed curves in (A) and (B) correspond to the $\bar{R}_h$ values from model $B_3$ and model $B_2$ samples, respectively. Dashed curve in (C) is obtained by displacing the model $B_2$ curve to the left in order to fit the dilution behavior of the native bile. Panel D shows dilution behavior of centrifuged native bile. Dashed curve is from model $B_3$.

quent decrease at precisely the same dilution factors $d_\gamma$ and $d_\alpha$ where the model system undergoes the micelle-to-vesicle transition.

In order to study the $1\alpha$ component more directly, we attempted to sediment component 2 from the $B_3$ bile sample using centrifugation methods and then perform dilution studies on the supernatant phase. After 4 h of centrifugation (20000*g*) the light scattering contribution by component 2 in the supernatant had been reduced to 4.7% (see section E). The influence of dilution on the $\bar{R}_h$ value of this sample (denoted $CF_4$) is shown in Figure 7D. The similarity between the centrifuged native bile and the dilution behavior of the model $B_3$ system is striking. This gives strong support to our previous data analysis of the uncentrifuged bile and offers unambiguous evidence for the "micellar identity" of the $1\alpha$ component.

In further dilution studies (data not shown) we have found that native bile samples $A_1$, $A_2$, $B_1$, and $C_1$ also exhibit the characteristic variation in $\bar{R}_h$ associated with the micelle-to-vesicle transition but that critical dilution factors $d_\gamma$ and $d_\alpha$ have different values in each case. Table III lists the critical dilution factors determined for all native bile samples studied. As expected from the phase diagram (Figure 4), the most concentrated A samples have the highest $d_\gamma$ and $d_\alpha$ values whereas the least concentrated C samples have the lowest. These trends are analyzed quantitatively in the following section.

Table III: Critical Dilution Factors and IMC Deductions

| sample | $(d_\gamma)_{exptl}$[a] | $IMC_\gamma$[b] | $(d_\alpha)_{exptl}$[c] | $IMC_\alpha$[d] |
|---|---|---|---|---|
| $A_1$ | 64 | 2.3 | 147 | 1.4 |
| $A_2$ | 45.2 | 2.5 | 104 | 1.6 |
| $B_1$ | 18.4 | 4.5 | 48.5 | 2.1 |
| $B_2$ | 10.5 | 6.2 | 26.0 | 3.3 |
| $B_3$ | 11.3 | 6.0 | 26 | 3.2 |
| $C_1$ | 13.9 | 2.9 | 32 | 1.7 |
| $C_2$ | 8.0 | 4.2 | 17.2 | 2.6 |

[a] Critical dilution factor corresponding to crossing of $\gamma$-boundary. [b] $IMC_\gamma$ deduced from $d_\gamma$ by using eq 5a. [c] Critical dilution factor corresponding to crossing of $\alpha$-boundary. [d] $IMC_\alpha$ deduced from $d_\alpha$ by using eq 5b.

*(3) IMC Deductions.* According to the equations defining the $\gamma$ and $\alpha$ phase boundaries (Mazer et al., 1980), the intermicellar BS concentrations $IMC_\gamma$ and $IMC_\alpha$ are related to the $d_\gamma$ and $d_\alpha$ values as follows:

$$IMC_\gamma = \frac{C^0_{BS} - \gamma^{-1}C^0_L}{d_\gamma} \quad (5a)$$

$$IMC_\alpha = \frac{C^0_{BS} - \alpha^{-1}C^0_L}{d_\alpha} \quad (5b)$$

where $\gamma$ is the L/BS ratio of mixed micelles formed in the coexistence regime and $\alpha$ is the L/BS ratio of the mixed disk bilayer. Using eq 5a,b in conjunction with the BS and L concentrations (Table I) and the $\gamma$ and $\alpha$ values for the TC–L system [$\gamma = 0.65$; $\alpha = 2.0$ at 20 °C (Mazer et al., 1980)], we have computed $IMC_\gamma$ and $IMC_\alpha$ for each sample (Table III).

For the B samples $IMC_\gamma$ and $IMC_\alpha$ are indeed close to the values of 6 and 3.2 mM found in model TC–L systems (Mazer et al., 1980) and are consistent with the results of Duane's (1977) equilibrium dialysis study of the TC–L system.

The lower values of $IMC_\gamma$ (2.4 mM) and $IMC_\alpha$ (1.5 mM) seen in the A samples are consistent with the presence of dihydroxy species in these "fasting" bile specimens. The latter value is in good agreement with Tamesue & Juniper's (1967) surface tension estimate of the "cmc" of human gallbladder bile, which is probably a measure of $IMC_\alpha$. Duane (1975) also studied human bile using the equilibrium dialysis method and found that the IMC depended on the L/BS ratio of the aggregates.[8] His values ranged from ~2.7 (L/BS ≈ 0.6) to ~1.2 mM (L/BS ≈ 2.0) and are remarkably close to our deductions of $IMC_\gamma$ and $IMC_\alpha$ in sample A.

Finally in the secretin-stimulated bile (sample C) the IMC values were intermediate between sample A and sample B, despite the expectation that they should be nearly the same as those of sample B. The origin of this difference is presently unclear but might involve subtle changes in the electrolyte composition of secretin-stimulated bile (Preisig et al., 1962) or the presence of bile salt species, other than taurocholate.

[8] Inadvertently some of Duane's data (1975) (L/BS ratio > 2.0) correspond to region III of the phase diagram where mixed vesicles (rather than micelles) are in equilibrium with BS monomers.

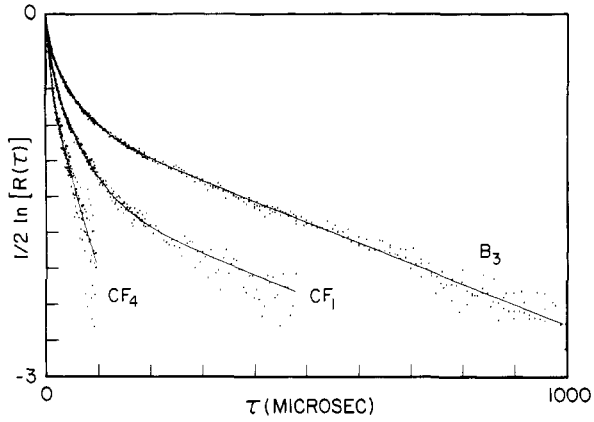


FIGURE 8: Spliced autocorrelation functions from sample $B_3$ and centrifuged samples $CF_1$ and $CF_4$, plotted as $^1/_2 \ln [R(\tau)]$ for values of $\tau$ between 0 and 1000 $\mu$s. Solid curve for $B_3$ is derived from the three-exponential fit. Solid curves for $CF_1$ and $CF_4$ are derived from an amplitude fit of the data by using diffusion coefficients derived from sample $B_3$ (see the text and Table IV for details).

*(D) Characterization of Component 1β: Calculated Contribution from Biliary Proteins.* As noted previously, the hydrodynamic radius of component 1β (~67 Å) falls in the range expected for the major serum proteins in dog bile (i.e., albumin and IgA), and it is reasonable to assume that the 1β component represents an average of these macromolecular species. Quantitative support for this view is provided by comparing the light scattering deductions of $R_{1\beta}$ and $G_{1\beta}$ (Table II) with calculations based on the sizes, molecular weights, and concentrations of the biliary proteins. On the basis of our own protein analysis of sample $B_3$ and the previous studies of Dive et al. (1974) we estimate that the concentrations of albumin and total IgA are both on the order of 0.2 g/dL in the B samples. Assuming that monomer, dimer, and tetrameric species of IgA are present in equal proportions, we calculate the mean hydrodynamic radius of the combined albumin/IgA fraction to be 72.5 Å, in good agreement with $R_{1\beta}$. By use of the same assumptions, the weight-averaged molecular weight of this fraction $\bar{M}_{1\beta}$ is found to be $\sim 2.19 \times 10^5$, roughly 20 times larger than the value calculated for the micellar component, $\bar{M}_{1\alpha} \sim 1.1 \times 10^4$ (see Appendix B). Taking the concentrations $C_{1\alpha} \sim 6$ g/dL and $C_{1\beta} \sim 0.4$ g/dL and the form factors $P_{1\alpha}$ and $P_{1\beta}$ as unity, the ratio of scattered intensity $G_{1\alpha}/G_{1\beta}$ is computed to be 0.75, in close agreement with the experimentally determined ratios on the B samples (~0.62; see Table II). Thus, both the size and relative scattering intensity of the 1β component are consistent with the contribution expected from the major biliary proteins in the dog.

*(E) Characterization of Component 2: Centrifugation Studies.* Centrifugation of sample $B_3$ for varying lengths of time (1–4 h) produces marked changes in the autocorrelation function $R(\tau)$ of the supernatant phases, as shown in Figure 8. With increasing centrifugation time, $R(\tau)$ exhibits a more rapid time decay, consistent with a reduced contribution from the large particles (component 2). A quantitative assessment of these changes was obtained by a three-exponential analysis of $R(\tau)$, in which the diffusion coefficients of the three species were taken to be the same as for components 1α, 1β, and 2 of sample $B_3$ (Table II), and only the amplitudes $G_{1\alpha}$, $G_{1\beta}$, and $G_2$ (equal to $1 - G_{1\alpha} - G_{1\beta}$) were allowed to vary. Such a two-parameter fit gave excellent agreement with the data (Figure 8) and thereby quantified the changes in the distribution of the three components produced by centrifugation. As seen in Table IV, the fractional intensity of component 2 decreases monotonically from 42% in sample $B_3$ to 4.7% in sample $CF_4$. The mean radius of all components likewise decreased monotonically from 30.5 to 17.9 Å.

Table IV: Amplitude Analysis of Centrifuged Bile

| sample[a] | $G_{1\alpha}$ (%)[d] | $G_{1\beta}$ (%)[d] | $G_2$ (%)[d] | $\bar{R}_{1\alpha+1\beta+2}$[e] |
|---|---|---|---|---|
| $B_3$ | 22.2 | 35.8 | 42.0 | 30.5 |
| $CF_1$[b] | 29.7 | 47.5 | 22.8 | 24.4 |
| $CF_2$[b] | 37.5 | 49.1 | 13.4 | 20.2 |
| $CF_3$[b] | 36.9 | 52.6 | 10.5 | 20.2 |
| $CF_4$[c] | 39.4 | 55.9 | 4.7 | 17.9 |

[a] Numeral in "CF" sample names denotes the number of hours centrifuged. [b] One-milliliter samples centrifuged in tubes with 9 mm i.d. [c] Four-milliliter sample centrifuged in tube with 15 mm i.d. [d] Fraction of scattered intensity associated with components 1α, 1β, and 2. [e] Mean hydrodynamic radius corresponding to 1α + 1β + 2 components on the basis of the intensity weighted average of diffusion coefficients.

These results show that only component 2 is sedimented from solution and that after 4 h at 20000*g*, nearly all of the large particles have been cleared from the supernatant. Since the sedimenting particles must travel a distance less than or equal to the inner diameter of the centrifuge tube (~1 cm) in order to reach and adsorb to the wall, it follows that their sedimentation velocity $V_s$ must be on the order of 1 cm/4 h or $7 \times 10^{-5}$ cm/s. This yields an estimate for the apparent sedimentation coefficient of component 2 of ~36 S.[9]

Combining this estimate with the measured diffusion coefficient of component 2, the Svedberg equation (Moore, 1962) implies that the apparent molecular weight of the large particles will be given by

$$M_2 = \frac{2.70 \times 10^6}{1 - \bar{v}_2 \rho_{\text{bile}}} \qquad (6)$$

where $\bar{v}_2$ is the partial specific volume of component 2 and $\rho_{\text{bile}}$ is the density of bile (estimated to be ~1.016 g cm$^{-3}$ from the solute constituents). If $\bar{v}_2$ is taken to be the same as for serum protein [i.e., ~0.73 cm$^3$ g$^{-1}$ (Tanford, 1961)], then eq 6 gives a value for $M_2$ of $1.0 \times 10^7$. From this, the equivalent spherical radius, $R_S$, would be ~147 Å, and the hydrodynamic asymmetry factor ($R_2/R_S$) would equal ~4.5, suggesting a markedly elongated and/or hydrated particle (Tanford, 1961) unlike any globular serum protein known to be present in native bile (Hardwicke et al., 1964; Dive et al., 1974; Mullock et al., 1978; Paul & Sreekrishna, 1979). These physical parameters are also incompatible with those known for gastric mucin glycoproteins (Pearson et al., 1980; Bloomfield, 1983) which are probably similar in structure to mucin proteins of the biliary tree.

On the other hand, if component 2 is assumed to be a spherical cell membrane vesicle, whose presence in bile has been postulated by Godfrey et al. (1981), then its molecular weight (including entrapped solvent) would be ~$7 \times 10^8$. Equation 6 would then imply that the partial specific volume $\bar{v}_2$ of component 2 would be ~0.980 cm$^3$ g$^{-1}$. This is indeed close to the partial specific volume determined for egg lecithin–cholesterol vesicles (Newman & Huang, 1975). Further evidence supporting the "vesicle assumption" is provided by the centrifugation and solubilization studies of Billington and co-workers (1978, 1980).

Although component 2 can be centrifuged from bile, we observed no visible sediment in any of our samples. In addition

[9] A more detailed analysis of the dependence of $G_2$ on centrifugation time (data of Table IV) gives virtually the same estimate for the sedimentation coefficient of component 2.

chemical analyses of the supernatants (including NaDodSO$_4$–PAGE on sample CF$_4$) showed no significant differences in biliary lipid, bilirubin, and protein content (quantitative or qualitative) from sample B$_3$. These "negative" findings, however, are consistent with the extremely low concentrations of component 2, estimated from the $W_2$ value (Table II) to be less than ~17 μg/mL. Differences of this size are too small to be detected by our analytical methods, and thus, a definitive chemical identification of component 2 remains to be achieved.

Finally, it should be noted that a particle of the same size and relative scattering intensity as component 2 has previously been detected by QLS in the gallbladder bile of prairie dogs (Mazer et al., 1979b). It may be significant that in both cases where such particles have been seen the major bile salt species present was taurocholate.

## Discussion

*Laser Light Scattering from Native Bile: The Three-Component Representation.* Although the presence of biliary pigments in native bile is a hindrance to laser light scattering experiments, it has nevertheless been possible in the present investigation to employ a scattering geometry which minimizes light absorption and thereby allows this technique to be effectively used for studying native bile.

From the autocorrelation functions of the scattered light, we have detected and characterized three macromolecular components (designated 1α, 1β, and 2) in hepatic bile samples from the dog. The major component, 1α, corresponds to greater than 90% of the total solute concentration and has a hydrodynamic radius ($R_{1\alpha}$) of ~10 Å, comparable in size to the $\bar{R}_h$ value (~15 Å) measured in aqueous biliary lipid solutions of identical composition. From the striking similarity of the effects of dilution on both model and native bile, proof of the micellar identity of the 1α component has been obtained. Component 1β accounts for ≲7.5% of solutes, and its hydrodynamic radius ($R_{1\beta}$) is ~67 Å. Calculations show that the size and scattering intensity of 1β are consistent with the "lumped" contribution expected from the principal serum proteins of bile, albumin, and IgA. Lastly, component 2 is a trace component (<0.03% of solutes) with a radius ($R_2$) of ~650 Å and a sedimentation coefficient of about ~36 S. At the present time indirect evidence suggests that these large particles may correspond to the canalicular membrane vesicles postulated by Godfrey et al. (1981) to be present in bile.

*Micelle-to-Vesicle Transition.* Dilution of model biliary lipid systems with physiological buffer produces dramatic changes in the distribution and sizes of micellar species and at high dilution induces the spontaneous formation of nearly monodisperse unilamellar vesicles (Mazer et al., 1980; Schurtenberger et al., 1983b). These changes can be understood as consequences of the partition equilibrium between bile salt molecules in the aqueous phase and those incorporated into micellar (or vesicle) structures. In effect, dilution draws bile salts away from the aggregates in order to reestablish the monomeric bile salt concentration (IMC) and thus increases the molar ratio of lecithin-to-bile salt (L/BS) remaining in the aggregate. Such variations in L/BS induce the growth of mixed disk micelles (Mazer et al., 1980) and also influence the size of bile salt–lecithin vesicles (Schurtenberger et al., 1983b).

By diluting native bile samples, we have observed changes in the behavior of the 1α component that are analogous to those seen in model bile solutions. This finding offers compelling evidence that bile salts, lecithin, and cholesterol form micellar aggregates in native bile whose sizes, structures, and equilibrium are quite similar to those in the model systems. Moreover, our results imply that biliary lipid interactions are not strongly influenced by the pigment and protein components present in native bile. The present work further demonstrates the usefulness of BS–L–Ch solutions as model systems for understanding the physical chemistry of bile (Carey & Small, 1978; Holzbach et al., 1973), consistent with the earlier success of the phase equilibria studies in rationalizing the presence or absence of cholesterol gallstones in man and other species (Admirand & Small, 1968; Redinger & Small, 1972).

*Previous Studies of Native Bile.* It is notable that some of the confusion and apparent contradiction in the earlier literature on native bile appears to be due to the influence of dilution on biliary lipid interactions and the existence of the micelle-to-vesicle transition. For example, the different "macromolecular properties" attributed to gallbladder and hepatic bile by Verschure et al. (Verschure & Hoefsmit, 1956; Verschure et al., 1956) were subsequently recognized (Norman, 1964a,b) to be consequences of the different total lipid concentrations, rather than the presence of any specific chemical factors produced in the gallbladder. Later bile studies using gel filtration chromatography (Thureborn, 1963; Niederhiser et al., 1964; Bouchier & Cooperband, 1967a,b) were also problematic since lecithin and cholesterol were separated from bile salts during passage through the column and appeared in the void volume as vesicles (Nalbone et al., 1973). In fact, the gel filtration method is now widely used to produce vesicles from micellar solutions of bile salt and lecithin (Brunner et al., 1976; Szoka & Papahadjopoulos, 1980). Recently, Reuben et al. (1982) studied rat bile with Sephadex columns that were equilibrated and eluted with different TC concentrations in order to prevent vesicle formation. Using protein markers, they found the apparent radius of the mixed micelles to vary from 16 Å in the presence of 40–60 mM TC to 35 Å in the presence of 4–5 mM TC. These sizes are comparable to those found in the present study and change in the direction expected from the phase diagram (Figure 4). Indirectly these studies also support the coexistence model in that simple TC micelles must be present at the TC concentrations used to equilibrate and elute the column. Similar conclusions can be inferred from the ultracentrifugation studies by Scharschmidt & Schmid (1978), who added 60 mM TC to their sucrose gradients.

From these examples it is clear that the aggregate structures formed in native and model bile are highly dependent on the biliary lipid concentrations and may be further altered by certain macromolecular methods. We believe that it is vital for investigators to be aware of these facts and to make use of the micellar phase diagram (Figure 4) in any attempts to characterize structure and equilibria in these systems.

*Pathophysiologic Implications.* The strong influence of total lipid concentration (i.e., dilution) on the aggregative behavior of native bile has potential physiologic relevance. In the course of digestion, duodenal bile can be diluted more than 30-fold (Sjövall, 1959), thereby inducing micellar growth and possibly vesicle formation (Stafford & Carey, 1981; Carey, 1982). These changes may have a direct influence on the rates of lipolysis (Weiloch, 1981) and the further solubilization and transport of hydrolytic products in the gut.

The micelle-to-vesicle transition may also be relevant to the mechanism of biliary lipid secretion. Greim et al. (1973) have found the intrahepatic concentration of bile salts to be ~0.04 mM, considerably smaller than IMC$_\alpha$. Thus, biliary lipid vesicles rather than micelles may be the species in which lecithin and cholesterol are transported *from* the endoplasmic reticulum of the hepatocyte *to* (and possible *across*) the

canalicular membrane.[10] Whether mixed micelles are formed in the canaliculus or distally in the biliary tree requires knowledge of the total lipid concentration in these locations, which is presently lacking. Nevertheless, it is well-known that the bile ductular system of the dog is capable of concentrating and diluting hepatic bile appreciably (Wheeler, 1972; Preisig et al., 1962) and therefore influences biliary lipid aggregation significantly within the biliary tree.

A final application of the micelle-to-vesicle transition concerns the formation of lipoprotein X, the abnormal serum lipoprotein seen in states of biliary obstruction. As is now appreciated (Hauser et al., 1977; Laggner et al., 1977; Brainard et al., 1980), lipoprotein X is a unilamellar vesicle ($R_h$ = 200–400 Å) containing biliary phospholipids, unesterified cholesterol, and small amounts of protein. It is conceivable that in the process whereby obstructed bile (or intrahepatic biliary lipids) refluxes into lymph and blood, bile salts could either be sufficiently diluted or become bound to other components such that a micelle-to-vesicle transition is induced.

In connection with component 2, our results provide indirect support for the hypothesis of Godfrey et al. (1981) concerning the presence of hepatocyte membrane vesicles in bile, derived from the canalicular microvilli. Nevertheless, as the component 2 particles represent an exceedingly small fraction of biliary solutes, their physiological significance remains to be established.

Finally, we believe that the present laser light scattering study of hepatic bile from the dog will provide useful information for future attempts to characterize normal and pathological human bile specimens with this technique. In this case, however, we anticipate that the presence of larger concentrations of cholesterol will lead to new aggregative phenomena (i.e., microdroplet formation, precipitation, etc.) that can likewise be compared with the behavior of model systems (Mazer & Carey, 1983; Stevens, 1977).[11]

Acknowledgments

We gratefully acknowledge the superb technical assistance of Hans Sägesser, who performed the bile collection experiments, Marco Wächter, who prepared model bile samples, and Olga Rösli, who typed the manuscript. Eva Niederer kindly assisted us with the centrifugation studies. Professor George Benedek (M.I.T.) and Clive Kuenzle (University of Zürich) made helpful suggestions, and Professor Björn Lindman (University of Lund) provided financial support for N.A.M. to attend the Fourth International Symposium on Surface and Colloid Science, Jerusalem, where portions of this work were presented. We also thank Dr. Pierre Wiltzius and Giovanni Dietler for helpful discussions and assistance with the computer analysis of the light scattering data and for pointing out the inexplicable similarity between Figure 7B and the Matterhorn.

## Appendix

*(A) Method for "Splicing" Autocorrelation Functions Together.* A set of $m$ autocorrelation functions $[C_1(\tau), C_2(\tau), \ldots C_m(\tau)]$ each measured at $N$ points ($\tau = T_i, 2T_i, \ldots NT_i$), where $T_i$ is the sampling time of the $i$th function, can be mathematically spliced together to yield a single normalized autocorrelation function $R(\tau)$, which decays from $R(0) = 1$ to $R(\infty) = 0$. Individually, each $C_i(\tau)$ is linearly related to $R(\tau)$:

$$C_i(\tau) = A_i R(\tau) + B_i \tag{A1}$$

where $A_i$ and $B_i$ correspond to the "true" amplitude and base line of the measured autocorrelation function. At identical $\tau$ values any two correlation functions are also related linearly [i.e., for $C_1(\tau)$ and $C_2(\tau)$]:

$$S_2^1 C_2(\tau) + I_2^1 \approx C_1(\tau) \tag{A2}$$

where the coefficients are given by

$$S_2^1 = A_1/A_2 \tag{A3a}$$

$$I_2^1 = B_1 - B_2(A_1/A_2) \tag{A3b}$$

Although $A_1$, $A_2$, $B_1$, and $B_2$ are not known a priori, $S_2^1$ and $I_2^1$ can be determined independently as follows. For $\tau^* = T_2$, $2T_2$, ... $kT_2$ (where $k$ is the greatest integer in $NT_1/T_2$) the values of $C_1(\tau^*)$ can be interpolated or taken directly from the measured values $C_1(jT_1)$, $j = 1, 2, \ldots N$. On the basis of eq A2, a least-squares line fit to the set of points $\{[C_2(\tau^*), C_1(\tau^*)]\}$ will have a slope and intercept corresponding to $S_2^1$ and $I_2^1$, respectively. With these values, all of the data points of $C_2(\tau)$ can be mapped onto a function $C_2^1(\tau)$ by using eq A2, and in this way a splicing of $C_2(\tau)$ to $C_1(\tau)$ is achieved. By a similar procedure the function $C_3(\tau)$ can be spliced to the combined functions $C_1(\tau)$ and $C_1^2(\tau)$ by using as many overlapping or interpolated points as possible. Extending this approach one can determine all of the splicing coefficients $S_j^1$, $I_j^1$ ($j = 2, 3, \ldots, m$) which are related to $A_j$, $B_j$ by the generalization of eq A3a,b:

$$S_j^1 = A_1/A_j \tag{A4a}$$

$$I_j^1 = B_1 - B_j(A_1/A_j) \tag{A4b}$$

The $A_j$, $B_j$ are determined from the splicing coefficients by using two boundary conditions related to the normalization of $R(\tau)$. The requirement that $R(\infty) = 0$ implies that for the last ($m$th) correlation function

$$C_m(\tau \to \infty) = B_m \tag{A5}$$

Thus, we can equate the experimentally determined base line of the $m$th function with the value of $B_m$. Equations A4a and A4b then permit all the remaining $B_j$ values to be solved. Similarly, the requirement that $R(0) = 1$ implies that

$$C_1(\tau \to 0) = A_1 + B_1 \tag{A6}$$

The value of $C_1(\tau \to 0)$ together with the previously determined value of $B_1$ permits $A_1$ to be calculated, and from the $S_j^1$ all of the other $A_j$ values can be computed. By use of $A_j$, $B_j$ thus determined, the functions $C_j(\tau)$ can each be mapped onto $R(\tau)$ by

$$[C_j(\tau) - B_j]/A_j \to R(\tau) \tag{A7}$$

*(B) Molecular Weights and Form Factors of Components 1α, 1β, and 2 (Case B).* The deductions of the $W_i$ values given in Table II (case B) were based on the following estimates of the molecular weights, $M_i$, and form factors, $P_i$, of the respective components.

| component | $M_i$ | $P_i$ ($\theta = 90°$) |
|---|---|---|
| 1α | $1.1 \times 10^4$ | 1 |
| 1β | $2.19 \times 10^5$ | 1 |
| 2 | $1.5 \times 10^8$ | 0.488 |

The estimate of $M_{1\alpha}$ is an average of the molecular weights of simple TC micelles ($\sim 2.69 \times 10^3$) and mixed TC–L mi-

[10] Such a mechanism is consistent with a recent mathematical analysis of biliary lipid secretion data (N. A. Mazer and M. C. Carey, unpublished results).

[11] Quite recently a QLS study of supersaturated human hepatic bile has been reported (Somjen & Gilat, 1983). Although not commented upon by the authors, there appears to be a definite similarity between their findings and the particle sizes measured in supersaturated model hepatic bile (Mazer & Carey, 1983).

celles ($\sim 2.4 \times 10^4$) weighted by the appropriate concentrations of each species as calculated for sample $B_3$ by using the model of simple and mixed micelle coexistence (Mazer et al., 1980). The estimate of $M_{1\beta}$ is likewise an average of serum albumin ($\sim 6.5 \times 10^4$) and IgA in the monomeric ($\sim 1.6 \times 10^5$), dimeric ($\sim 3.2 \times 10^5$), and tetrameric states ($\sim 6.4 \times 10^5$). It assumes the same concentration (0.2 g/dL) for albumin and total IgA [consistent with the range of concentrations measured for these proteins in dog bile (Dive et al., 1974)] and divides the latter equally among the three IgA species. The form factors for $1\alpha$ and $1\beta$ are taken as unity in view of their small hydrodynamic radii (<100 Å). In the case of component 2, $M_2$ is estimated for a membrane vesicle with outer radius 663 Å and inner radius 613 Å assuming a partial specific volume of 1 $cm^3\ g^{-1}$. This neglects the weight of the solvent entrapped within the vesicle (which does not contribute to the scattered intensity) and is therefore smaller than the value of $M_2$ obtained from eq 6. The value of $P_2$ is estimated from the Guinier formula [i.e., $\exp(-q^2Rg^2/3)$, using $Rg$ = 640 Å).

**Registry No.** Cholesterol, 57-88-5; sodium taurocholate, 145-42-6; bilirubin, 635-65-4.

References


Admirand, W. H., & Small, D. M. (1968) *J. Clin. Invest. 47*, 1043.

Bartlett, C. R. (1959) *J. Biol. Chem. 234*, 466.

Bertero, M., & Pike, E. R. (1983) in *Photon Correlation Techniques in Fluid Mechanics* (Schulz-DuBois, E. O., Ed.) p 298, Springer-Verlag, Berlin.

Bevington, P. R. (1969) in *Data Reduction and Error Analysis for the Physical Sciences*, McGraw-Hill, New York.

Billington, D., & Coleman, R. (1978) *Biochim. Biophys. Acta 509*, 33.

Billington, D., Evans, C. E., Godfrey, P. P., & Coleman, R. (1980) *Biochem. J. 188*, 321.

Bloomfield, V. A. (1983) *Biopolymers 22*, 2141.

Bouchier, I. A. D., & Cooperband, S. R. (1967a) *Clin. Chim. Acta 15*, 291.

Bouchier, I. A. D., & Cooperband, S. R. (1967b) *Clin. Chim. Acta 15*, 303.

Brainard, J. R., Cordes, E. H., Gotto, A. M., Patsch, J. R., & Morrisett, J. D. (1980) *Biochemistry 19*, 4273.

Brunner, J., Skrabal, P., & Hauser, H. (1976) *Biochim. Biophys. Acta 512*, 147.

Carey, M. C. (1982) in *The Liver: Biology and Pathobiology* (Arias, I. M., et al., Eds.) p 429, Plenum Press, New York.

Carey, M. C., & Small, D. M. (1970) *Am. J. Med. 49*, 590.

Carey, M. C., & Small, D. M. (1978) *J. Clin. Invest. 61*, 998.

Carey, M. C., Montet, J.-C., Phillips, M. C., Armstrong, M. J., & Mazer, N. A. (1981) *Biochemistry 20*, 3637.

Chu, B. (1974) in *Laser Light Scattering*, Academic Press, New York.

Claffey, W. J., & Holzbach, R. T. (1981) *Biochemistry 20*, 415.

Cotlove, E., Trantham, H. V., & Bowman, R. L. (1958) *J. Lab. Clin. Med. 51*, 461.

Dive, C., Nadalini, R. A., Vaerman, J.-P., & Heremans, J. F. (1974) *Eur. J. Clin. Invest. 4*, 241.

Duane, W. C. (1975) *Biochim. Biophys. Acta 398*, 275.

Duane, W. C. (1977) *Biochem. Biophys. Res. Commun. 74*, 223.

Ford, J. R., & Chu, B. (1983) in *Photon Correlation Techniques in Fluid Mechanics* (Schulz-DuBois, E. O., Ed.) p 303, Springer-Verlag, Berlin.

Godfrey, P. P., Warner, M. J., & Coleman, R. (1981) *Biochem. J. 196*, 11.

Greim, H. P., Czygan, P., Schaffner, F., & Popper, H. (1973) *Biochem. Med. 8*, 280.

Haller, H. R. (1980) Dissertation (6604), ETH, Zürich, Switzerland.

Hardwicke, J., Rankin, J. G., Baker, K. J., & Preisig, R. (1964) *Clin. Sci. 26*, 509.

Haslewood, G. A. D. (1967) in *Bile Salts*, Methuen & Co. Ltd., London.

Hauser, H., Kostner, G., Müller, M., & Skrabal, P. (1977) *Biochim. Biophys. Acta 489*, 247.

Holzbach, R. T., Marsh, M., Olszewski, J., & Holan, K. (1973) *J. Clin. Invest. 52*, 1467.

King, J., & Laemmli, U. K. (1971) *J. Mol. Biol. 64*, 465.

Koppel, D. E. (1972) *J. Chem. Phys. 57*, 4814.

Laggner, P., Glatter, O., Müller, K., Kratky, O., Kostner, G., & Holasek, A. (1977) *Eur. J. Biochem. 77*, 165.

Laurell, C. B. (1966) *Anal. Biochem. 15*, 42.

Lowry, O. H., Rosebrough, W. J., Farr, A. L., & Randall, R. J. (1951) *J. Biol. Chem. 193*, 265.

Mazer, N. A. (1984) in *Dynamic Laser Scattering: Applications of Photon Correlation Spectroscopy* (Pecora, R., Ed.) Plenum Press, New York (in press).

Mazer, N. A., & Carey, M. C. (1983) *Biochemistry 22*, 426.

Mazer, N. A., Benedek, G. B., & Carey, M. C. (1976) *J. Phys. Chem. 80*, 1075.

Mazer, N. A., Carey, M. C., & Benedek, G. B. (1977) in *Micellization, Solubilization and Microemulsions* (Mittal, K. L., Ed.) Vol. 1, p 359, Plenum Press, New York.

Mazer, N. A., Carey, M. C., Kwasnick, R. F., & Benedek, G. B. (1979a) *Biochemistry 18*, 3064.

Mazer, N. A., Lee, S. P., Carey, M. C., & Benedek, G. B. (1979b) *Gastroenterology 76*, 1197 (Abstract).

Mazer, N. A., Benedek, G. B., & Carey, M. C. (1980) *Biochemistry 19*, 601.

Mazer, N., Schurtenberger, P., Carey, M., Känzig, W., & Preisig, R. (1981) *Gastroenterology 80*, 1314 (Abstract).

Michaëlsson, M., Nosslin, B., & Sjölin, S. (1965) *Pediatrics 35*, 925.

Missel, P. J., Mazer, N. A., Benedek, G. B., Young, C. Y., & Carey, M. C. (1980) *J. Phys. Chem. 84*, 1044.

Moore, W. J. (1972) *Physical Chemistry*, Prentice-Hall, Englewood Cliffs, NJ.

Müller, K. (1981) *Biochemistry 20*, 404.

Mullock, B. M., Dobrota, M., & Hinton, R. H. (1978) *Biochim. Biophys. Acta 543*, 497.

Nakayama, F. (1969) *J. Lab. Clin. Med. 73*, 623.

Nalbone, G., Lafont, H., Domingo, N., Lairon, D., Pautrat, G., & Hauton, J. C. (1973) *Biochimie 55*, 1503.

Neiderhiser, D. H., Roth, H. P., & Webster, L. T. (1964) *J. Clin. Invest. 43*, 1252 (Abstract).

Newman, G. C., & Huang, D. H. (1975) *Biochemistry 14*, 3363.

Norman, A. (1964a) *Proc. Soc. Exp. Biol. Med. 115*, 936.

Norman, A. (1964b) *Proc. Soc. Exp. Biol. Med. 116*, 902.

Ostrowsky, N., & Sornette, D. (1983) in *Photon Correlation Techniques in Fluid Mechanics* (Schulz-DuBois, E. O., Ed.) p 286, Springer-Verlag, Berlin.

Paul, R., & Sreekrishna, K. (1979) *Indian J. Biochem. Biophys. 16*, 399.

Paumgartner, G., Horak, W., Probst, P., & Grabner, G. (1971) *Naunyn-Schmiedebergs Arch. Pharmakol. 270*, 98.

Pearson, J., Allen, A., & Venables, C. (1980) *Gastroenterology 78*, 709.

Preisig, R., Cooper, H. L., & Wheeler, H. O. (1962) *J. Clin. Invest. 41*, 1152.

Putnam, F. W. (1965) in *The Proteins—Composition, Structure and Function* (Neurath, H., Ed.) Vol. 3, Academic Press, New York.
Redinger, R. N., & Small, D. M. (1972) *Arch. Intern. Med. 130*, 618.
Reuben, A., Howell, K. E., & Boyer, J. L. (1982) *J. Lipid Res. 23*, 1039.
Sanders, A. H., & Cannell, D. S. (1980) in *Light Scattering in Liquids and Macromolecular Solutions* (Degiorgio, V., Corti, M., &. Giglio, M., Eds.) Plenum Press, New York.
Scharschmidt, B. F., & Schmid, R. (1978) *J. Clin. Invest. 62*, 1122.
Schurtenberger, P., & Mazer, N. A. (1981) *Helv. Phys. Acta 54*, 626 (Abstract).
Schurtenberger, P., Mazer, N. A., & Känzig, W. (1983a) *J. Phys. Chem. 87*, 308.
Schurtenberger, P., Mazer, N. A., Känzig, W., & Preisig, R. (1983b) in *Proceedings of the International Symposium on Surfactants in Solution (Lund 1982)* (Mittal, K. L., & Lindman, B., Eds.) Plenum Press, New York (in press).
Sjövall, J. (1959) *Acta Physiol. Scand. 46*, 339.
Small, D. M., Penkett, S. A., & Chapman, D. (1969) *Biochim. Biophys. Acta 176*, 178.
Somjen, G. J., & Gilat, T. (1983) *FEBS Lett. 156*, 265.
Spink, C. H., Müller, K., & Sturtevant, J. M. (1982) *Biochemistry 21*, 6598.
Stafford, R. J., & Carey, M. C. (1981) *Clin. Res. 29*, 511 A.
Stevens, R. D. (1977) *J. Lipid Res. 18*, 417.
Szoka, F., & Papahadjopoulos, D. (1980) *Annu. Rev. Biophys. Bioeng. 9*, 467.
Tamesue, N., & Juniper, K. (1967) *Gastroenterology 52*, 473.
Tanford, C. (1961) in *Physical Chemistry of Macromolecules*, Wiley, New York.
Thomas, J. E. (1941) *Proc. Soc. Exp. Biol. Med. 46*, 260.
Thureborn, E. (1963) *Nature (London) 197*, 1301.
Verschure, J. C. M., & Hoefsmit, F. M. C. (1956) *Clin. Chim. Acta 1*, 38.
Verschure, J. C. M., Mijnlieff, P. F., Hoefsmit, F. M. C., & Van Der Moeven, A. E. N. (1956) *Clin. Chim. Acta 1*, 154.
Weigand, K., Schmid, M., Villringer, A., Birr, Ch., & Heinrich, P. C. (1982) *Biochemistry 21*, 6053.
Weiloch, T. (1981) Doctoral Thesis, University of Lund, Sweden.
Wheeler, H. O. (1972) *Arch. Intern. Med. 130*, 533.
Wheeler, H. O., & King, K. K. (1972) *J. Clin. Invest. 51*, 1337.

# Reduction of Cytochrome Oxidase by 5,10-Dihydro-5-methylphenazine: Kinetic Parameters from Rapid-Scanning Stopped-Flow Experiments†

Folim G. Halaka,‡ Zexia K. Barnes, Gerald T. Babcock, and James L. Dye*

ABSTRACT: The kinetics of the reduction of resting cytochrome oxidase and of its cyanide complex by 5,10-dihydro-5-methylphenazine (MPH) have been characterized by rapid-scan and fixed-wavelength stopped-flow spectrophotometry in the Soret, visible, and near-IR spectral regions. In this study, we focused on a form of the resting enzyme that is characterized by a Soret absorption maximum at 424 nm. These experiments complement earlier work on the reduction of a 418 nm absorbing form of the resting enzyme [Halaka, F. G., Babcock, G. T., & Dye, J. L. (1981) *J. Biol. Chem. 256*, 1084–1087]. The reduction of cytochrome *a* is accomplished in a second-order reaction with a rate constant of $3 \times 10^5$ $M^{-1}$ $s^{-1}$. The reduction of the 830-nm absorber, $Cu_a$, is closely coupled to but lags the reduction of cytochrome *a*; we have resolved a rate constant of about 20 $s^{-1}$ for the copper reduction. The reduction of cytochrome *a* proceeds with a rate constant that is nearly independent of the spectral properties of the resting enzyme and of the ligation state of cytochrome $a_3$. The reduction of cytochrome $a_3$ occurs by slow, intramolecular electron transfer. We have resolved two phases for this process that have rate constants of $\sim$0.2 $s^{-1}$ and $\sim$0.02 $s^{-1}$ for both the 418- and 424-nm forms of the resting enzyme. It appears, therefore, that spectroscopic heterogeneity at the cytochrome $a_3$ site in the resting enzyme exerts very little influence on the kinetics of the anaerobic reduction of the oxidase metal centers. From this we conclude that the rate of electron transfer to the $a_3$ site is probably controlled by the protein conformation and not primarily by local factors within the $a_3$ environment.

Redox reactions are of central importance to the understanding of the catalytic activity of cytochrome *c* oxidase in electron transport. In biological systems, the enzyme catalyzes the four-electron reduction of molecular oxygen to water [for reviews see Malmström (1979) and Wikström et al. (1981)]. The reduction of the protein, either under anaerobic conditions or during turnover in the presence of oxygen, has been extensively studied, particularly by using its natural substrate, cytochrome *c* [for example, Gibson et al. (1965), Andreasson et al. (1972), Andreasson (1975), Wilms et al. (1981) and Antalis & Palmer (1982)]. The reduction of the oxidase has also been carried out by using the positively charged metal ion complexes hexaaquochromium(II) (Greenwood et al., 1977) and hexaammineruthenium(II) (Scott & Gray, 1980; Reichardt & Gibson, 1982) and by using the negatively charged species $SO_2^{-}\cdot$ (Halaka et al., 1981). Those studies suggest that the charge type of the reductant plays an important role in the kinetics of reduction and in determining the site of interaction with the oxidase.

A second conclusion that has been drawn from this earlier work is that the rate of intramolecular electron transfer from

† From the Department of Chemistry, Michigan State University, East Lansing, Michigan 44824-1322. *Received August 18, 1983; revised manuscript received December 6, 1983.* This research was supported by NSF Grant PCM 78-15750 (J.L.D.) and NIH Grant GM 25480 (G.T.B.).
‡ Present address: A. A. Noyes Laboratory of Chemical Physics, California Institute of Technology, Pasadena, CA 91125.

0006-2960/84/0423-2005$01.50/0 